Trans. JWRI, Vol. 25(1996), No.2

Modelling of Viscosity and Fluid Dynamics in Similar Friction Joints

G.J. Bendzsak and T.H. North

Department of Metallurgy and Materials Science
University of Toronto

Abstract

The purpose of this paper is to describe an approximate mathematical model for studies of steady state, non-Newtonian flow regimes within friction welds. The complex flow patterns are described by a numerical solution of the Navier-Stokes equations which relies upon a heuristic model for viscosity. The results obtained predict many features observed in the micrographs of experimental samples. Three main topics are discussed in the paper. The first relates to a method of estimation for the parameters of a non-Newtonian viscosity model for the base material. The second concerns the retention of particles, and of the flow itself, within the weld zone. The third illustrates that the theoretical framework predicts the existence of spiral defects.

1. Introduction

It has been shown that the friction welding process can be characterised as a number of distinct stages[1]. The purpose of this paper is to present a mathematical framework for the steady state period of the process. The main thrust is a description of a theoretical approach to the modelling of fluid flow, and retention of both base material and impurities within the weld zones of similar materials[2]. It is known that the mechanical properties of joints depend on the ejection of contaminants such as oxide debris from the weld region and it has been pointed out that the forging operation cannot by itself remove contamination retained at the bondline[3]. The fundamental assumption of the paper is that after a brief start-up period, the weld zone is both thermally and mechanically in steady-state, and the final forging stage only captures, but does not alter, the situation existing at the end of this period.

In the present paper, the Navier-Stokes equations are used to investigate the characteristics of the non-Newtonian flow at the contact zone. It is worth indicating that although the friction welding process has been modelled by a number of investigators[4-8], until recently[2] no prior research has been specifically aimed at providing an understanding of fluid flow behaviour at the bondline region of friction welded joints. At the present state of research, there exist a number of uncertainties and unknown quantities which render the present mathematical model to be a first approximation to the steady-state period of the welding process.

2. Analytical Formulation

Formulation of the analytical framework consists of a number of steps leading to a numerical model which accounts for the effects of geometry, viscosity, non-Newtonian flow and the dynamics of particles trapped within the

Transactions of JWRI is published by Joining and Welding Research Institute of Osaka University, Ibaraki, Osaka567, Japan.

flow. The joint is assumed to be isothermal.

2.1 Rheology of the flow region

Rheology is a well established science[9], but relevant data for the non-Newtonian relationships required for solution of the present problem are not available. Since standard viscosity measurement techniques are difficult to apply, *a heuristic approach* is used to establish approximate values for the parameters of a steady state, isothermal apparent viscosity model for the aluminium base taking into account shear thinning. Consequently, parameters of a rheological model which account for the dependency of viscosity on the histories of temperature and sheer rate[9] are not required. The viscosity model presented in this paper predicts both power requirements and magnitude of the isothermal temperature within a steady state flow region. The validity of the proposed model is justified by the agreement between a number of experimental and theoretical results.

In general, viscosity is dependent upon temperature, shear and normal stresses and may be represented by the functional form:

$$\mu = f(\tau, T, P_a) \qquad (1)$$

where: μ=viscosity; τ= shear stress; T = temperature; P_a = applied pressure. During the steady-state stage in the friction welding operation, the temperature in the weld zone can be assumed to be isothermal while the axial force is maintained constant. Consequently, the apparent viscosity μ_a can be considered as a function of the shear stress alone, with the effect of shear thinning approximated by the simple empirical formula[10]:

$$\mu_a = \mu_\infty + (\mu_0 - \mu_\infty)\exp(-B\tau_{r\theta}) \qquad (2)$$

where: μ_∞ = viscosity of liquid base material; μ_0 = reference viscosity; B = constant; $\tau_{r\theta}$ = shear stress. The value of μ_∞.; has a negligible magnitude in comparison with μ_0. Thus Eqn. (2) is simplified to:

$$\mu_a = \mu_0 \exp(-B\tau_{r\theta}) \qquad (3)$$

The two constants μ_0 and B are characteristic of the material, in our case aluminium, and are normally determined by experiment. Given the experimental difficulties, these have been estimated through an iterative method based on the equivalence between the total mechanical power delivered to the weld zone and its complete viscous dissipation by the single component fluid. The final values of these constants for aluminium alloy base material are μ_0 = 5000 Pa-s, and B = $0.5*10^{-8}$

The relationship between shear stress and shear rate is:

$$\tau_{r\theta} = \mu_a \frac{dV_\theta}{dz} \qquad (4)$$

where: V_θ = rotational velocity; z = axial distance. The variations of viscosity and shear rate with shear stress are shown respectively in **Fig. 1**a and Fig. 1b.

The steady state welding temperature for an aluminum base material is estimated to be in the order of 540℃ At this temperature, the values of viscosity change only due to sheer thinning with the approximate values between 2500 and 4500 poise. Under such an operating condition, the base material can be thought of as a high viscosity fluid, and while global melting of the base material is not required for joining, the above model does not exclude the possibility of localized melting along grain boundaries as shown in **Fig. 2**.

2.2 Width of the flow region

The numerical solutions of the flow patterns within a friction weldjoint place a heavy burden on computational facilities. Consequently, it would be advantageous to confine, a priori, the flow within a pre-defined region. In steady state, a relationship can be derived for such bounds through the consideration of balance between the mechanical energy and its dissipation by viscous effects.

The applied force in the axial direction is given by:

$$F_a = \amalg R_o^2 P_a \qquad (5)$$

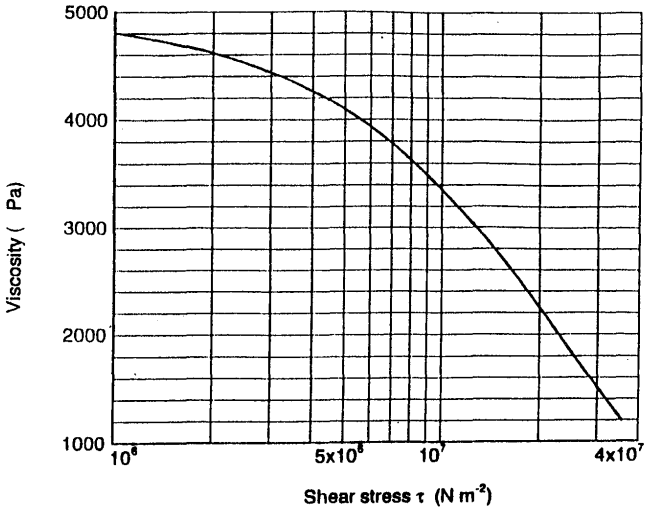

Figure 1a Viscosity as function of sheer stress.

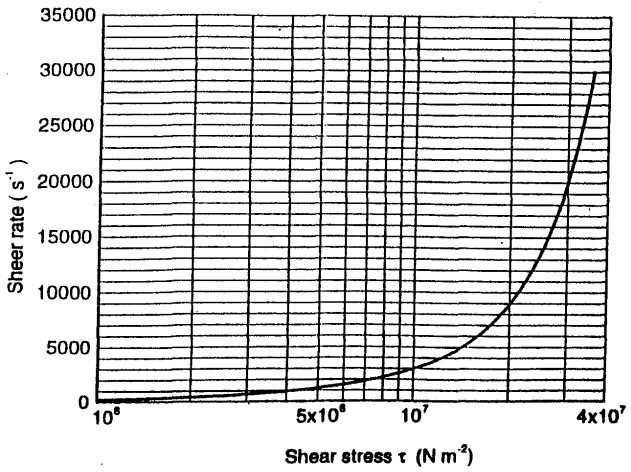

Figure 1b Shear rate as function of sheer stress.

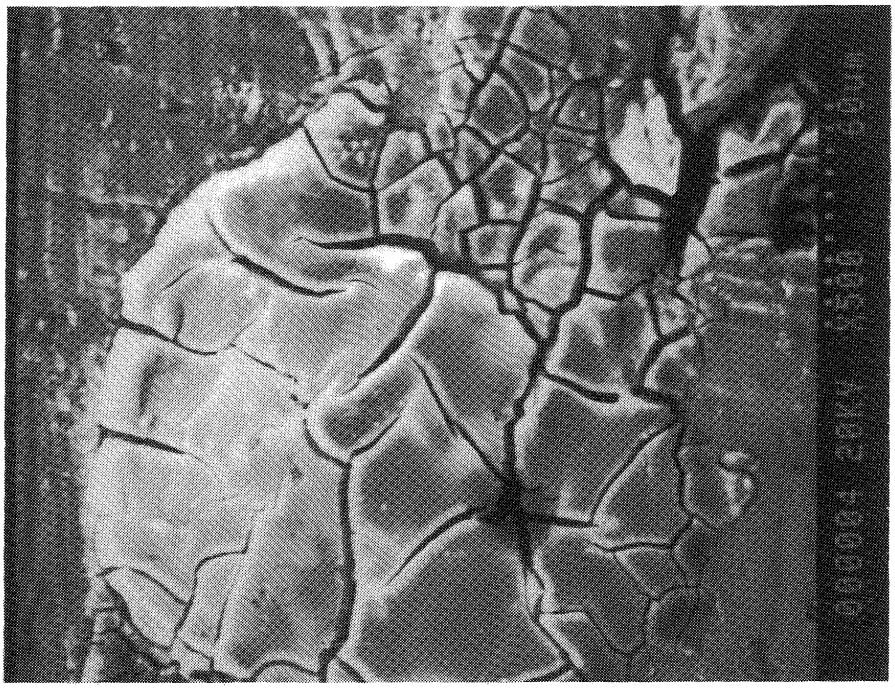

Figure 2 Hot cracking in a region at the periphery of an MMC/MMC joint.

where: F_a = applied axial force; R_0 = outside radius. This results in a delivered mechanical power density:

$$P_{ar} = \eta \frac{R_o^2 P_a \omega}{2rh(r)} \qquad (6)$$

where: η = coefficient of friction; ω = rotational speed; r = radial distance; h(r) = width of flow region. The shear rate is an approximate function of the radius, hence the density of viscous power dissipation, $P_{\mu d}$, is given by:

$$P_{\mu d} = \mu\Phi^2 = \mu\left(\frac{r\omega}{h(r)}\right)^2 \qquad (7)$$

In steady state Eqn.(6) and Eqn. (7) are equal giving a relationship for h(r), the width of the flow region as function of radial position:

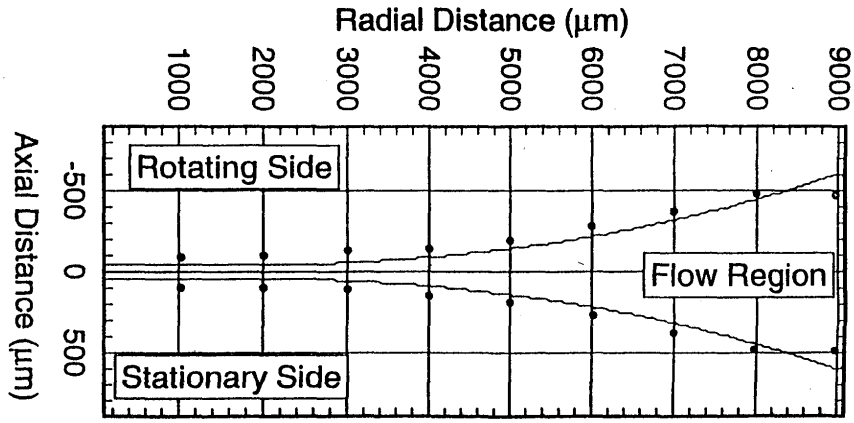

Figure 3 Theoretical and experimental widths of the flow region. The line is obtained from Eqn. 8 and the dots are measured values for Aluminium base material.

TABLE I Operating Conditions and MMC Material Properties.

Operating Parameters			**Aluminium MMC Properties**	
Process Parameter	**Values**		**Quantity**	**Magnitude**
Original Radius	9 mm		Density	2700 kg/m^3
Speed of rotation	1500 rpm		Thermal conductivity	250 W/m ^{0}C
Pressure - steady state - forging	30 MPa 30 MPa		Viscosity	Non-Newtonian relationships are shown in Figure 1b
Weld Duration	4.5 sec			
Axial Speed	2.5 mm/sec			

$$h(r) = \mu \frac{2r^3\omega}{\eta R_o^2 P_a} \qquad (8)$$

The relationship for h(r) takes into account the non-Newtonian characteristics of viscosity, as given by Eqn. 3 . Predicted and corresponding measured variation of h(r) are shown in **Fig. 3** for an 18mm diameter aluminium alloy base material for the experimental conditions given in **Table I** .

The generally good agreement along the radial direction underlies the validity of the viscosity model described in Section2.1. The principle differences between experimental measurements and the theoretical relationship of Eqn. 8 is due to the lack of power generation along the line of symmetry, resulting in h(0)=0. In actual weld joints, thermal conduction assures that such a condition does not occur. In spite of this problem, Eqn. 8 predicts the joint width well for radii larger than 3000 μ m and the theoretical values are in agreement with other experimental results[3,8].

The problem of zero zone width in the vicinity of the axis of symmetry was eliminated by a simple 60 μ m extension of the region for radial distances less than 3000 μ m. Equation 8 can be used to estimate the average width of the weld zone resulting in an effective value for sheer stress.

2.3 An Estimate for the Weld Joint Temperature

The assumption of isothermal conditions within the weld joint can be now tested by a simple one dimensional model for temperature distribution along the effective thermal length of the workpiece. In the friction welding machine used to obtain the experimental results, both rotating and stationary pieces are firmly secured by heavy steel grips which form large heat sinks. Thus, the effective thermal length of each piece is in the order of 25 mm. Analysis of the steady state temperature behaviour in the axial direction is simplified by the high value of thermal diffusivity for the aluminium base material, and the low values of radiation and convective heat losses at the outer radius. The distribution of temperature is a function of axial distance from the weld joint and is independent of radius. Heat generation in the joint is assumed to be confined to a region having an average width obtained from Eqn. 8

$$H_{avg} = \mu \frac{R_o^2 \omega}{2\eta P_a} \qquad (9)$$

A steady state temperature solution within the flow region can be estimated by considering a region having a width as specified by Eqn. 9 and an average power density of pg. The temperature rise in the zone is given by:

$$\Delta T = \frac{P_g H_{avg}^2}{2k} \qquad (10)$$

In the regions external to the flow, the temperature variation is given by:

$$T = \frac{P_g H_{avg}}{k}(L - z) + T_a \qquad (11)$$

where: L = effective thermal length (25mm), k=thermal conductivity, Ta=ambient temperature. In order to reach a temperature of 540℃, the dissipated power in the weld joint is approximately 1622W. The corresponding maximum temperature deviation as given by Eqn. 5 is less than 5℃. Thus, the result of this simple ID analysis supports the isothermal hypothesis of Section 2.2

2.4 Estimation of Flow Velocity along the Radial Boundary

The axial force applied during the steady-state period extrudes material on either side of the contact zone and imposes a outward directed flow. The magnitude of the velocity could be obtained from a full solution of the equations of plastic deformation. However, it is thought that a reasonable velocity estimate can be obtained from the solution of a potential problem in either viscoplastic region. Mass continuity is maintained, and expulsion of material through small annular openings adjacent to the boundaries account for the formation of the flash. Their widths are set equal to the mean value at the base of the flash at R_0=9000μm. The flow field is given by Eqn. 12.

$$U = \nabla \times \Psi \qquad (12)$$

where: **U** = velocity vector; ∇ = Laplacian operator; Ψ = stream function. Since the flow is irrotational it must satisfy the equation of continuity i.e. $\nabla \cdot \mathbf{U} = O$, then vector relationship becomes:

$$\nabla \times U = \nabla \times \nabla \times \Psi = \nabla^2 \Psi = \mathbf{0} \qquad (13)$$

The boundary conditions for the Laplace's equation (13) take into account the conservation of mass, symmetry and the outflow of material through an annulus of width **W**.

Eqn. (13) was solved for a number of cases taking into account variations in geometry, velocity and **W**. An averaged relationship between the normalized radial velocity$_v$ and radius r, for the region 1.0 mm < **W** < 3.0 mm, is shown in **Fig. 4**. It will be shown below that the interpretation of the result of Fig. 4 along the boundary specified by Eqn. 8 leads to different flow configurations observed in friction welding.

2.5 Governing Equations for the Flow Region

Having defined functions for the apparent viscosity of the fluid and the steady state boundary of the weld region, the behaviour of flow is governed by the equations of Navier-

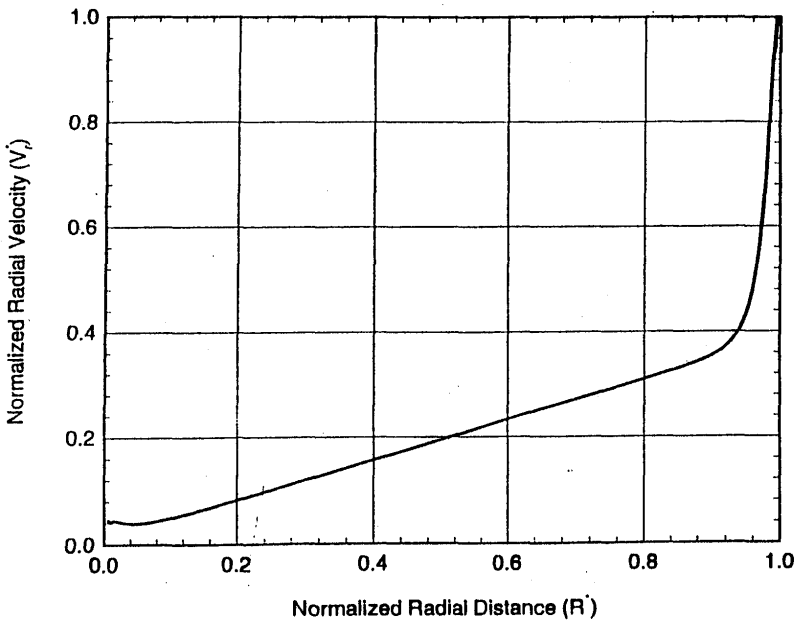

Figure 4 Normalized averaged radial velocity along the stationary and rotating surfaces.

Stokes and continuity. The problem is symmetric in the angular direction, consequently the velocity components are functions of the radial (r) and axial (z) dimensions only. Under these conditions the governing equations are:

$$\rho\left(v_r\frac{\partial v_r}{\partial r}-\frac{v_\theta^2}{r}+v_z\frac{\partial v_r}{\partial z}\right) = -\frac{\partial p}{\partial r}+\mu\left[\frac{\partial}{\partial r}\left(\frac{1}{r}\frac{\partial}{\partial r}(rv_r)\right)+\frac{\partial^2 v_r}{\partial z^2}\right] \quad (14)$$

$$\rho\left(v_r\frac{\partial v_z}{\partial r}+v_z\frac{\partial v_z}{\partial z}\right) = -\frac{\partial p}{\partial z}+\mu\left(\frac{1}{r}\frac{\partial}{\partial r}\left(r\frac{\partial v_z}{\partial r}\right)+\frac{\partial^2 v_z}{\partial z^2}\right) \quad (15)$$

$$\rho\left(v_r\frac{\partial v_\theta}{\partial v_r}+\frac{v_r v_\theta}{r}+v_z\frac{\partial v_\theta}{\partial v_z}\right) = \mu\left(\frac{\partial}{\partial r}\left(\frac{1}{r}\frac{\partial}{\partial r}(rv_\theta)\right)+\frac{\partial^2 v_\theta}{\partial z^2}\right) \quad (16)$$

$$\frac{1}{r}\frac{\partial}{\partial r}(\rho r v_r)+\frac{\partial}{\partial z}(\rho v_z)=0 \quad (17)$$

where: ρ = density of fluid; v_r= radial component of velocity; v_θ = angular component of velocity; v_z= axial component of velocity. These relationships form a set of coupled two dimensional, second order, nonlinear partial differential equations which can be solved only numerically.

There are a number of numerical techniques available for the solution of the Navier Stokes equations. These are principally differentiated by the treatment of pressure and geometry[11]. It has been found that a control volume formulation based upon the Semi-Implicit Method for Pressure Linked Equations of Patankar (**SIMPLE**) is particularly robust, hence it was selected as the preferred solution technique. Detailed description of this methodology is presented in Reference[12]. The flow is fully laminar since the Reynolds number, based on the outer radius of the workpiece and the lowest value of dynamic viscosity, is in the order of 0.014.

The velocity boundary condition along the line of demarcation between the flow region and the adjoining viscoplastic zones is given by the relationship of Fig. 4 which can be interpreted in one of two ways:

a) The boundaries given by Eqn. 8 are essentially expanding in the radial direction. If the flow obtained from the potential problem of Eqn. 13 is fullyradial, then material must freely enter and leave through these boundary maintain continuity (Eqn. 17). The solution is essentially quasi-static since there is no growth in the radial direction.

b) The relationship of Fig. 4 represents a tangential variation of velocity along the boundary. Under this condition, material exchange across the boundaries do not occur but the momentum is allowed to vary in the prescribed fashion.

These boundary conditions lead to two families of solutions which have been observed experimentally.

The remaining boundary conditions concern those along the centre and outer radius. These involve symmetry along the centreline and free slip at the outer radius (R_0) of the flow region. The rotational boundary conditions are $V_\theta = 0$ and $V_\theta = r\omega$ along the stationary and rotating surfaces. Once a numerical solution has been obtained for the flow region, values for of the dependent parameters can be readily calculated. These include the shear stress, the shear rate, the apparent viscosity, and the power absorbed by viscous dissipation.

3. Theoretical results for basic flow features

3.1 Flow due to purely radial extrusion

Reference[2] describes in detail the results obtained by the solution of the Navier-Stokes equation subject to the first interpretation of Section 2.5. In this paper, these are now summarized for the operating conditions given by Table I. In the discussion below the radial growth of the flow region is represented by a quasi steady-state evolution at an estimated rate of 250μm/sec from an originally undeformed radius of R_0=9000μm to a final R_0=9900μ m as shown in **Fig. 5** a through Fig. 5d.

The salient features of the analysis are:

a) Base material leaves through the narrow annular area located immediately adjacent to the rotating surface at R_0, where the radial velocity is positive in the outward direction.

b) Along the outer radius R_0, and small distances from both stationary and rotating boundaries, v_r and v_z, are both negative in the axial direction and material is continuously returned from the stationary surface to wards a plane normal to the axis of rotation.

c) The material supplied from the viscoplastic regions by a process of advection. The radially increasing flow either returns to the adjacent regions or leave through the surface at R_0.

d) The flow pattern can be divided into two distinct zones:

i) Zone 1: where the non-Newtonian fluid is driven in the radial direction with mass being supplied from the adjacent viscoplastic layers. At radii between 8000μm and 8800μm, the axial component of the flow field reverses and some of the advected material is returned to the viscoplastic regions. The remainder is expelled through the annular area next to the rotating interface.

ii) Zone 2: where the direction of boundary velocity is parallel to the rectangular extrusion zone. A flow is induced by shear, changing the essentially radial motion into that of recirculation.

e) The transition from radial flow to recirculation is smooth over an approximate distance of 1000μm. Material at R_0 is extruded over an approximate axial distance of 200μm from both the stationary and rotating boundaries.

f) At a radial distance of 8250μm from the centreline, all radial and axial components of velocity become zero due to matter arriving from all radial directions which is diverted axially towards either the rotating or stationary surface. This corresponds to the formation of a mathematical saddle point representing a fundamental change in flow characteristics.

g) The dynamics of small particles can be studied by computing the motions of infinitesimal masses released at several locations within the flow region. The results of a streamtrace analysis are shown in **Fig. 6** a through Fig. 6d for the theoretical flow conditions described above.

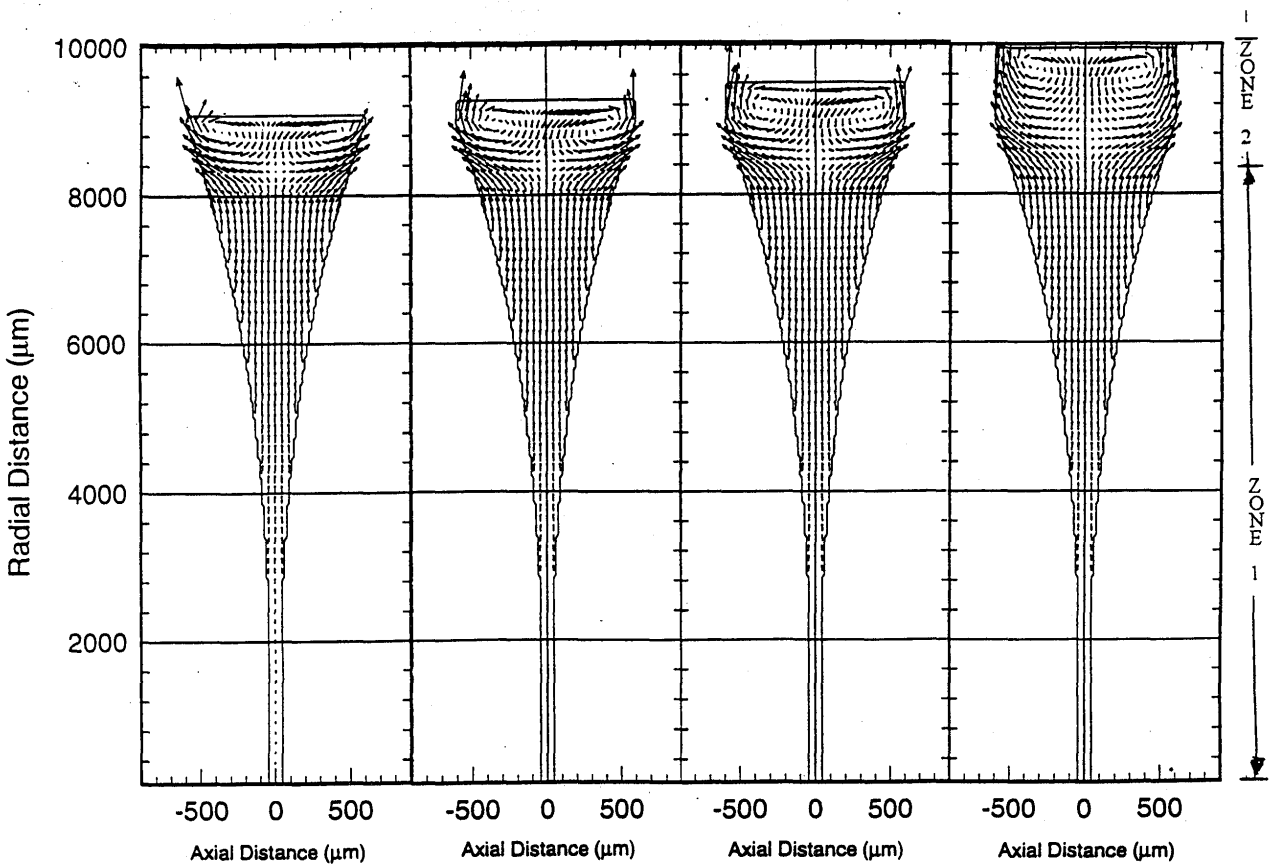

5a) Original Radius R_o=9000μm 5b) 220 μm Extension 5c) 440 μm Extension 5d) 900 μm Extension

Figure 5 Evolution of flow in radial direction from the original radius at R_0=9000μm to its final position at R_0=9900 μm

h) An examination of Fig. 6 shows that the streamtraces cross each other during the radial expansion of the weld. The presence of a point of bifurcation and the crossing streamtraces can be associated with the unstable and/or chaotic phenomenon of fluid mixing[13]. This observation leads to the suggestion that the weld strength of similar materials could be related to a mixing index.

i) The flow Reynolds number is low, hence particle paths coincide with those of the streamtraces.

j) In Zone 2, an exchange of particles occurs between the stationary and rotating surfaces resulting in particle depletion on the stationary side and a corresponding increase in particle density on the rotating side of the joint.

k) The presence of singularities in the flow are responsible for the crowding of streamtraces towards the flow boundaries. When the tracer particles approach the joint periphery, they are either deflected, or trapped, by one of two re-circulating regions.

1) The aluminium base material within the weld zone is confined by the flow and is prevented from leaving everywhere, except for small regions near the boundaries, for the following reasons:

i) rotational flow in the weld is always in the same direction,
ii) depending on the location within the weld, the radial velocity component can assum directions either away from or towards the centreline. Thus, the direction of a vector formed by the radial and angular velocity

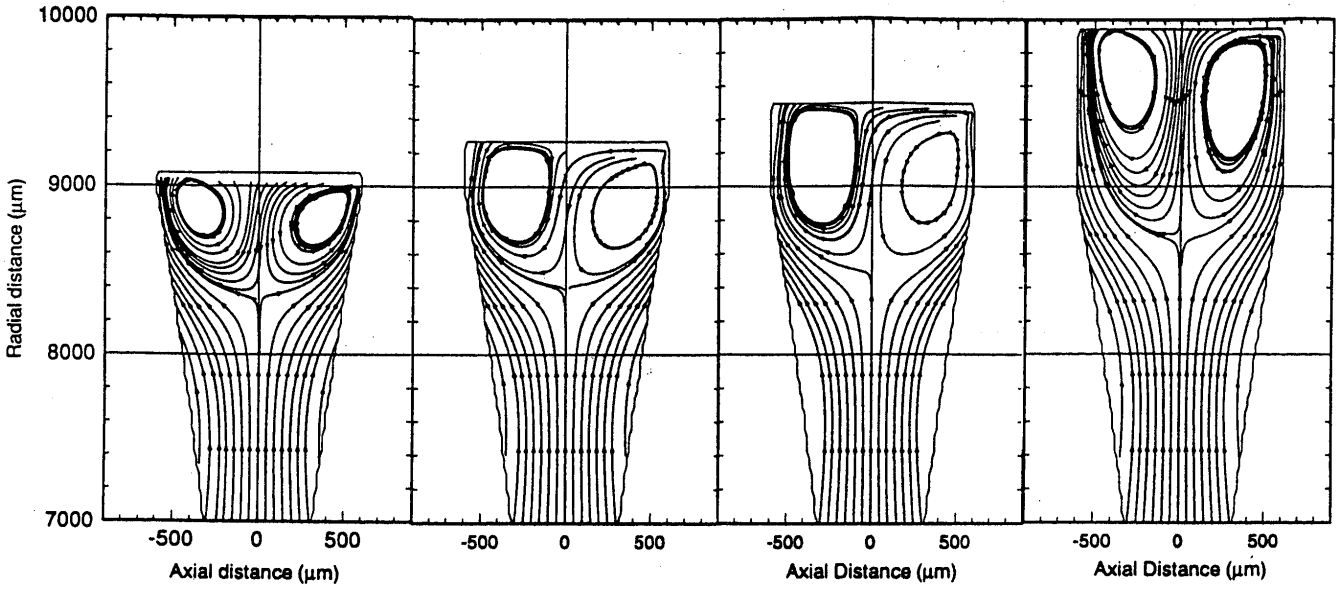

6a) Original Radius R_o=9000μm

6b) 220 μm Extension

6c) 440 μm Extension

6d) 900 μm Extension

Figure 6 Streamtraces corresponding to the flow fields of Figure 5.

components must change somewhere alon the radius. In regions radially outwarddirected flow, base material spirals towards the outside, with the reverse being true for the radially inward directed flow regions,

iii) a neutral plane is formed at the point of zero radial velocity. Base material on both sides of this plane spiral towards this attractor and becomes retained during the welding operation.

m) As a consequence of the combination of low Reynolds number and Point 1) above, particles become entrapped in the weld joint and can never be removed completely. Due to the presence of re-circulating regions they are squeezed against the flow boundaries where they accumulate in time. Furthermore, a depletion process from the stationary side of the joint encourages a higher particle density along the rotating side.

It should be noted that the streamtrace patterns shown in the diagrams would be only realized inpractice, if and only if , the welding process is allowed to continue for the conditions of a period ofinfinite duration, fixed geometry, and the absence of instability. The duration of friction welding is finite, the weld zone expands radially, and an instability is created by the saddle point. Therefore, the theoretical framework presented above is only but a first step in the analysis of a complex mixing phenomenon occurring during the steady-state period of friction welding.

4. Comparison Between Theoretical and Experimental Results

4.1 Experimental results

An experimental procedure for flow visualization within friction weld joints is described in Reference[2] along with a number of microsections supporting the findings of the analysis described above. Typical overall flow pattern in the weld joint is shown in **Fig. 7.** The principle common features between experimental and theoretical results are:

a) the hour-glass shaped flow regions which are approximately symmetrical with respect to the axis of rotation,

b) the division of the flow into two zones along the radial direction showing signs of a

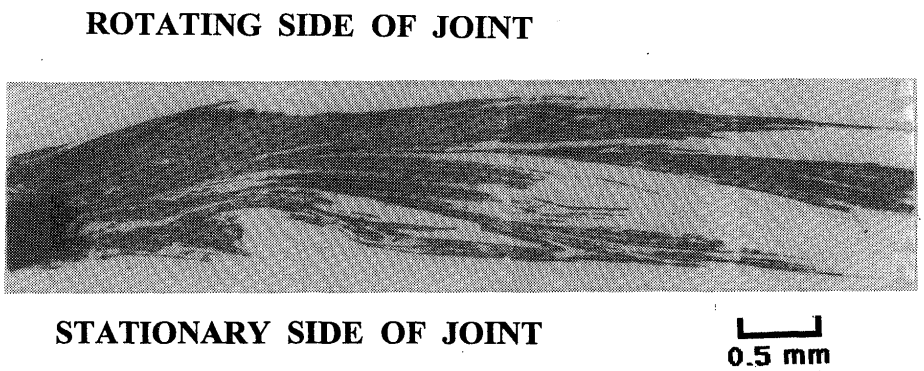

Figure 7a Flow patterns indicating splitting, large areas of folding, and stretching.

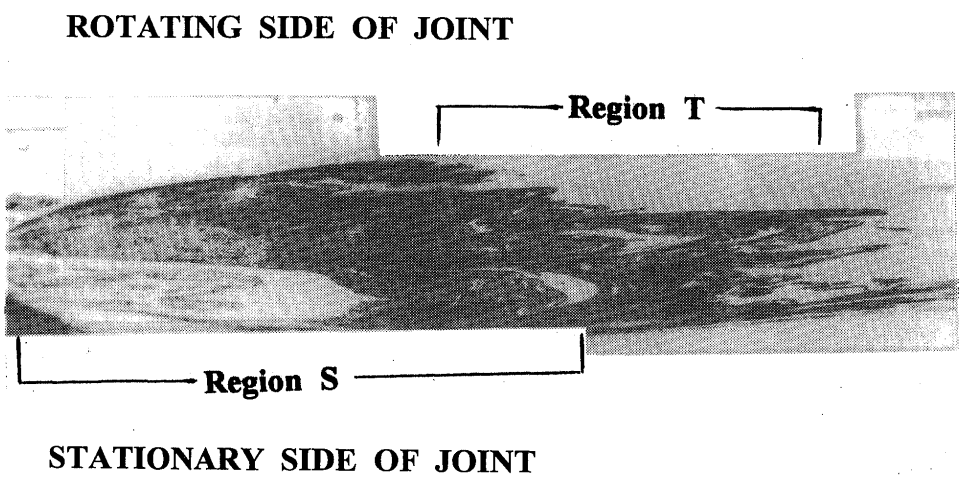

Figure 7b Flow patterns indicating large areas of re–circulation, some stretching, and folding.

circulatory flow (Fig. 7b) and the presence of unstable "ramming" and "splitting" of the flow by radial infusion of material (Fig. 7a),

c) an agreement between the key features of the experimental and calculated flow patterns, indicating the capability of the numerical model to predict the general features of fluid flow during welding,

d) evidence of particle concentration and folding near the rotating surface is observed in Region T of Fig. 7b and clear re-circulation is seen on the stationary side within Region S,

e) an enlarged area of the rotating side of Fig. 6b is shown in Fig. 7 for the neighbourhood R = 9000 μ m. The micrographs in Fig. 7 show the concentration of particles along the boundary. The alumina trace particles were uniformly distributed in the test specimens prior to welding, hence their preferential concentration at the calculated positions can be taken as one confirmation of the overall validity of the mathematical approach. The alignment of particles with the flow also indicate the correctness of the assumption that they follow closely the streamtraces. Thus, the experimental evidence supports the suggestion that the particles follow paths predicted by the steady-state model for the entrapment and retention of impurities within the friction welded joint.

f) the complexity and richness of the experimental flow suggests a break-up of the theoretical patterns by the mechanism of instability,

The differences between the experimental and theoretical results show that the model fails to predict the complex structures and

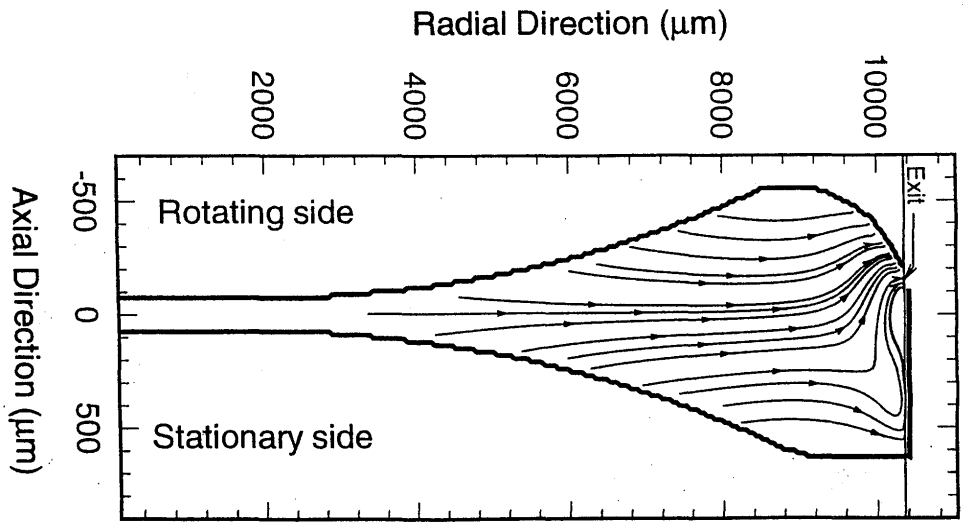

Figure 8 Effect of curvature of the rotating boundary upon calculated flow characteristics.

the radially outward directed flows on the rotating side. The first feature is associated with the point of bifurcation which is responsible for the creation of chaotic flow in the weld. The second aspect can be resolved by taking into account the curvature of the rotating boundary.

4.2 Effect of boundary curvature on flow characteristics

The velocity vectors near the outer radius R_0 and the rotating boundary are directed towards the central plane as shown in Fig. 5a through Fig. 5d. This flow pattern should produce a curved boundary between the flow region and the adjacent rotating viscoplastic material. This curvature is indeed observed in the micrographs of Fig. 7. The assumptions within the present model exclude the possibility of predicting the shape of the flow region towards the outer radius of the weld joint. However, the geometry of can be easily modified to take into account the effect of this curvature. This is achieved by arbitrarily adjusting he shape of the rotating boundary to resemble that observed in an actual weld by gradually reducing the width of flow region by 40% in the vicinity of the outer radius R_0, The shape of the stationary boundary was left intact.

The resulting streamtraces are shown in **Fig. 8**. The limit cycle on the rotating side is eliminated and the flow in this region becomes radial in agreement with the experimental results. The point of bifurcation is retained, and is shifted radially outwards. An enlarged view of the flow in the vicinity of R_0 is shown in **Fig. 9b** and a comparison of the calculated and experimental flow patterns are in reveals excellent agreement.

5. Flow due to tangential extrusion velocity

Solution of the Navier-Stokes equation subject to the second interpretation of radial described in Section 2.5 produces the dramatically different flow pattern shown in **Fig. 10** below. When the flow streamtraces of this result are compared to that of Fig. 6a, it is seen that:

a) the dynamics of the flow are comparable in the half region adjacent to the rotating side. The recirculating region towards the outer radius is retained to squeeze the flow patterns against the boundary,

b) the point of bifurcation along the centre line of the weld is absent,

c) a series of spiral arms appear near the stationary boundary. The widths of these arms are between 10μm and 30μm in the axial direction. Their radial spacings vary between 150μm and 250μm.

d) each arm exhibits its own spiral which attract particles and effectively trap them within the joint,

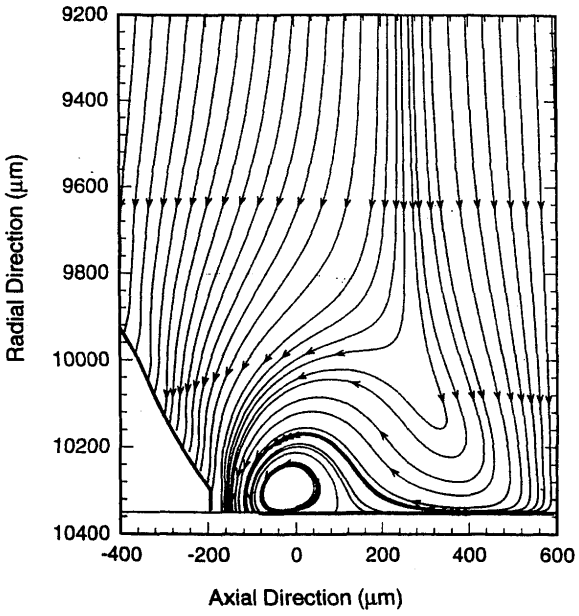

Figure 9a Calulated flow pattern.

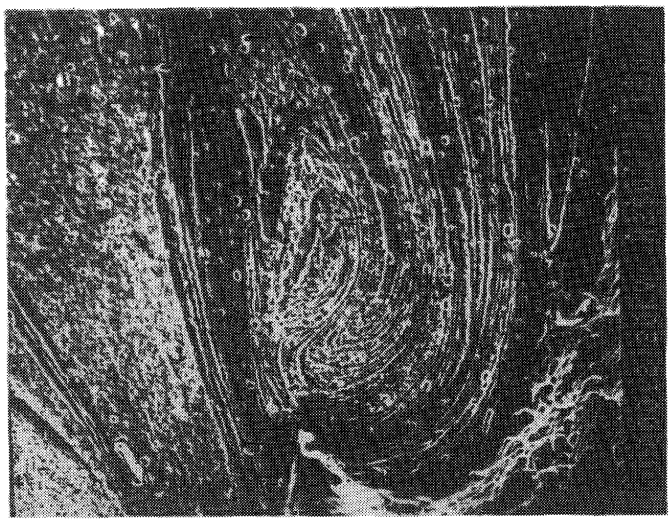

Figure 9b Enlarged view of Figure7b.

Figure 9 Calculted and experimental flow patterns in the vicinity of the outer radius.

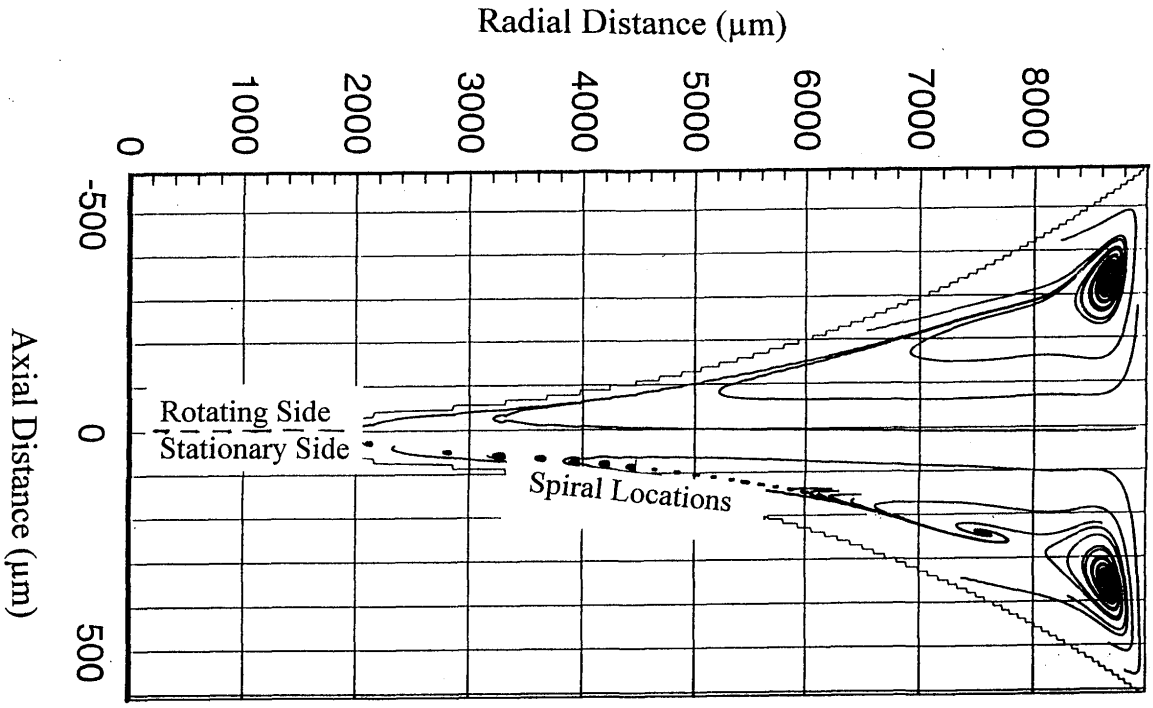

Figure 10 Development of spiral arms in the vicinity of the stationary side.

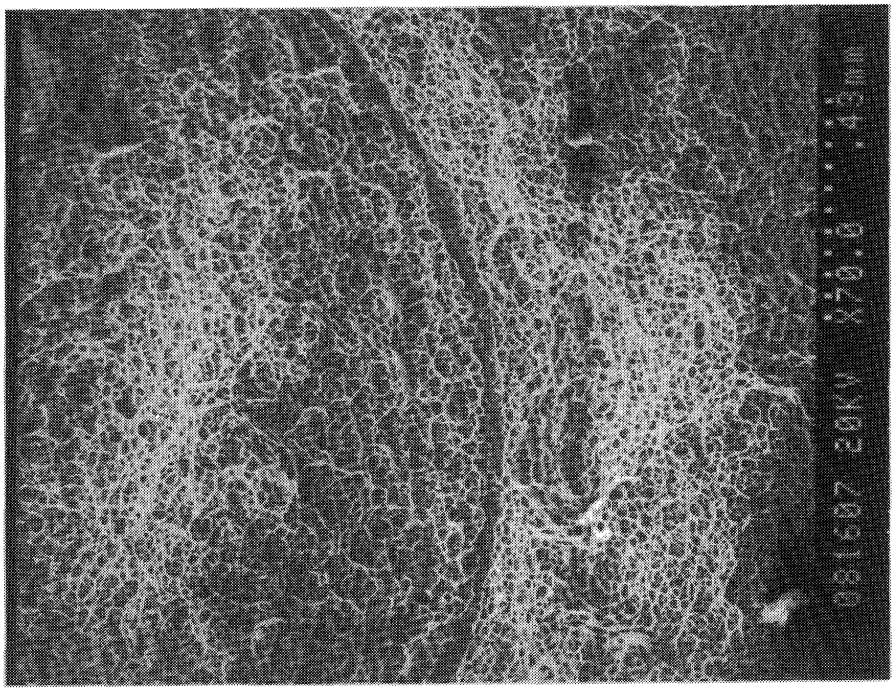

Figure 11 Experimental evidence for spiral arms in the vicinity of the stationary side.

e) the large recirculating zone on the stationary side of the flow is retained.

Fig. 11 shows a spiral armwhose features are in general agreement with those observed experimentally. The flow mechanism leading to this phenomenon is thought to be related to the dissipation of vorticity within the flow. The results of Fig. 10 and Fig. 11 have been included in this paper to illustrate the ability of the model to predict spiral defect. A full investigation of this effect is the subject of a publication in preparation.

6. Conclusions

The major conclusions of this paper are as follow:

a) The standard equations of fluid dynamics can be used to describe flow behaviour within the joints of friction welding. Their numerical solution show a chaotic and unstable flow which is responsible for mixing of base material in the joint.

b) A consideration of balance between power generation and its dissipation in the weld region leads to an analytical formula for the width of the flow regime as a function of radius.

c) Under isothermal conditions, a non-Newtonian viscosity model can be derived from heuristic arguments. During the steady state period of friction welding, by taking into account sheer thinning, the power dissipated by viscous dissipation can be approximated to reasonable accuracy.

d) The flow patterns predicted by the numerical model depend upon the nature of the extrusion process and the geometry of the weld region.

e) Large numbers of particles are retained and become segregated in specific locations within the joint. Particle accumulation is most apparent at the interface between the flow region and the rotating workpiece. Significant numbers of particles line up with the flow and become trapped along unstable streamtraces.

f) The model successfully predicts the presence of spiral defects.

The theoretical and experimental results lead to the overall conclusion that the bonding

mechanism during friction welding can be visualized in terms of a mixing process of a creeping, single component, non-Newtonian flow. While the first order solution presented in this paper provides useful information regarding fundamental mechanisms, a more full description of the details of this mixing awaits more work. Accordingly, the results of this study should be looked upon only as a first step in the prediction of bond strength from first principles.

Acknowledgments

The authors would like to thank the Ontario Center for Materials Research and Hatch Associates Ltd. for their support of this work.

References

1) O.T. Midling and O. Grong, Acta metall. 42,1595 (1994)
2) G.J. Bendzsak, T.H. North, and Z. Lee (Paper excepted for publication in Acta Mater.), 1996
3) T. Rich and R. Roberts, Weld. J. 3, 137s (1971)
4) A. Francis and R.E. Crane, J. Heat Mass Transfer 28, 1747 (1985).
5) N.N. Rykalin, A.J. Pujin and V.A. Vaasiljeva, Weld. Prod. 42, 6 (1959).
6) J.J. Healy, D.J. McMullin and A.S. Bahrani, Wear 37, 265 (1976).
7) A. Sluzalec and A. Sluzalec, Int. J. Heat and Mass Transfer 36, 1583 (1993).
8) K.K. Wang and P. Nagappan, Weld. X49, 419s (1970).
9) S. Peter, Chem. Ing. Tech. 32, 437 (1960).
10) R.S. Brodkey, The Phenomena of Fluid Motions, Dover Publications, 388, (1995)
11) W.J. Minkowycz, E.M. Sparrow, G.E. Schneider, R.H. Pletcher, Handbook of Numerical Heat Transfer, Wiley, (1988).
12) S.V. Patankar, Numerical Heat Transfer and Fluid Flow, Hemisphere Publishing, (1980).
13) J.M. Ottino, The Kinematics of Mixing: Stretching, Chaos, and Transport, Cambridge University Press, Cambridge, (1989).